SIN-CHN SCIENTIFIC PRESS PTE.LTD.

Molecular & Cellular Biomechanics 2025, 22(4), 1648.
https://doi.org/10.62617/mcb1648

Article

Intelligent navigation systems: Adaptive endoscopic navigation strategies for complex intestinal environments by combining the biomechanics

Xinyu Ma[1], Jinyang Gao[1,*], He Huang[2], Jingyao Zhang[1], Chenzhi Lu[1], Guozheng Yan[3]

[1] State Key Laboratory of Dynamic Measurement Technology, North University of China, Taiyuan 030051, China
[2] Department of Gastrointestinal Surgery, First Hospital of Shanxi Medical University, Taiyuan 030001, China
[3] School of Biomedical Engineering, Shanghai Jiaotong University, Shanghai 200240, China
*** Corresponding author:** Jinyang Gao, gjy.1001@163.com

CITATION

Ma X, Gao J, Huang H, et al. Intelligent navigation systems: Adaptive endoscopic navigation strategies for complex intestinal environments by combining the biomechanics. Molecular & Cellular Biomechanics. 2025; 22(4): 1648. https://doi.org/10.62617/mcb1648

ARTICLE INFO

Received: 21 February 2025
Accepted: 4 March 2025
Available online: 17 March 2025

Abstract: The advancement of endoscopic visual navigation is critical for accurate diagnosis and treatment of colonic disease. However, traditional techniques face challenges in adaptability to complex colonic conditions. This is exemplified by their limited ability to respond effectively to different situations, which results in less accurate navigation planning. This study proposes a navigation system to overcome this issue and improve navigation adaptability. An adaptive strategy has been designed based on a multidimensional discrimination method to guide endoscopes in traversing complex colonic environments. This strategy takes into account the biomechanical properties of the colon, such as tissue flexibility and kinematic characteristics, enhancing navigation accuracy. Furthermore, specific strategies for calculating navigation points have been developed for colonic collapses and tumors to ensure effective navigation under various biomechanical conditions. In simulated tests for the colon model, the system achieved an overall success rate of 92.5% (multiple scenarios), with average deviations of 3.15 mm horizontally and 2.51 mm vertically. Additionally, the system is characterized by its ease of operation, thereby reducing the reliance on operational experience and protracted training. By combining the principles of biomechanics, this study not only improves the accuracy of endoscopic navigation but also provides a new perspective for the treatment of colon diseases and emphasizes the importance of biomechanics in clinical applications.

Keywords: navigation; intelligent system; biomechanics; computer-assisted navigation; adaptive strategy

1. Introduction

Intestinal diseases pose a significant threat to human health [1]. According to the 2022 global cancer data [2], colorectal cancer is the third most common cancer in the global cancer incidence rate, accounting for 9.6% of all cancer cases, with a mortality rate of 9.3% among the fatal cases. Early screening and diagnosis are crucial for reducing treatment costs and improving the quality of patient survival [3,4]. As medical technology progresses, endoscopy emerges as a pivotal diagnostic tool in the timely detection and treatment of colorectal diseases due to its minimally invasive nature and high effectiveness [5].

The differences in endoscopic operation skills are an important factor affecting the quality of colonoscopy [6]. Traditional colonoscopy requires manual navigation of the endoscope through the intricately curved colon, requiring the skill and expertise of the surgeon [7]. However, the complex structure of the human colon and individual differences make endoscopy prone to contact or friction with the colonic wall. This

issue can increase patient discomfort and severe complications. Extended procedures can also lead to physician fatigue, compromising examination accuracy and safety [7]. Recent studies [8] have underscored the necessity of delivering consistent, efficient, and high-quality endoscopy services, emphasizing the imperative to enhance examination safety and patient comfort. The advent of computer-aided navigation technologies offers a potential solution to this challenge [9]. In particular, visual navigation technology employs image processing techniques to process image data from endoscopic sensors and computational tools, thereby assisting physicians in operating endoscopes with greater precision and reducing the reliance on physician operating experience. Navigation systems can facilitate endoscopic operations even for those with limited experience [10], thereby enhancing the accuracy and efficiency of operations, reducing the likelihood of complications, and improving the patient experience and quality of examinations.

Perceiving the environment from endoscopic images is a critical aspect of the navigation [11]. Given the colonoscopy's complexity, there is an urgent need for more robust and reliable visual navigation techniques. Researchers are actively exploring navigation methods. Reilink et al. [12], Xia et al. [13], and Zhang et al. [14] utilized the dark-area method of navigation, in which the endoscope is guided forward by searching for dark areas in the image. However, the dark areas in the lumen image are vulnerable to light interference. Furthermore, the proximity of the light source to the tube lumen wall results in an overall brighter image, causing the dark areas to be less visible or disappear, invalidating the dark area method. Another approach is the optical flow method, explored by Liu et al. [15] and Stap et al. [16], which is based on the principle of balancing the size of the optical flow at each feature image point and achieves navigation at locations with greater cavity curvature. However, the method's sensitivity diminishes in the straight rows region of the lumen. Ciuti et al. [17], Abu-Kheil et al. [18], Floor et al. [19], and Onogi et al. [20] extracted 3D information based on 2D-lumen images and reconstructed the lumen for navigation. However, the reconstruction error rate is high and time-consuming due to the small number of feature points and regional variability in the lumen. Jiang et al. [21] attempted to overcome these limitations by combining the dark area method with the optical flow method to realize the navigation at any position in the colonic lumen. Nevertheless, the utilization of a single judgment criterion, namely the presence of a dark area, is inadequate to accommodate the complexity of the colonic environment and to make optimal navigational decisions, which may lead to increased deviation.

This study proposes an adaptive navigation strategy to address this issue. This strategy employs a multidimensional discriminative method to guide endoscopes through complex colonic environments, thereby improving endoscopic navigation's adaptive capability in complex environments. The key contributions of this study are as follows:

1) A comprehensive discriminative mechanism based on quantitative analysis of image features is proposed to analyze various complex situations in the endoscopic navigation process in a multidimensional way and to select the optimal navigation strategy. The accuracy of the calculation of navigation points is enhanced.

2) The calculation strategy of navigation points is proposed for the special cases of colonic collapse and tumor, enhancing the adaptability of endoscopic navigation in

special environments. Colonic collapse, specifically refers to the closure or partial closure of the lumen of the colon (a part of the large intestine) due to insufficient internal pressure and reduced gas or contents. Commonly seen during colonoscopy, caused by underinflation or abnormal bowel wall tension.

2. Method of navigation

2.1. Design of dark area method

The autonomous guidance system developed by Krishnan et al. [22] demonstrates the possibility of utilizing depth information to enable automated navigation of an endoscope through the human colon.

The endoscope relies exclusively on the camera to capture image information of the colon. A point light source illuminates the colonic wall; the light source and the camera on the endoscope can be considered to be situated in approximately the same plane. As the light source approaches the object, the light no longer appears parallel but instead becomes reflected. The correlation between the light intensity at the reflection point and the distance from the light source to the reflection point in the colonic wall can be described as follows.

$$I_{inc} \propto \frac{I_0}{r^2} \tag{1}$$

where I_{inc} is the light intensity at the reflection point and r is the distance from the light source to the reflection point at the colonic wall. Here, I_0 is the light intensity of the light source. Since the light source and the camera are positioned closely together, the deepest part of the colon corresponds in the image to the darkest place of the colon, considering the observation angle.

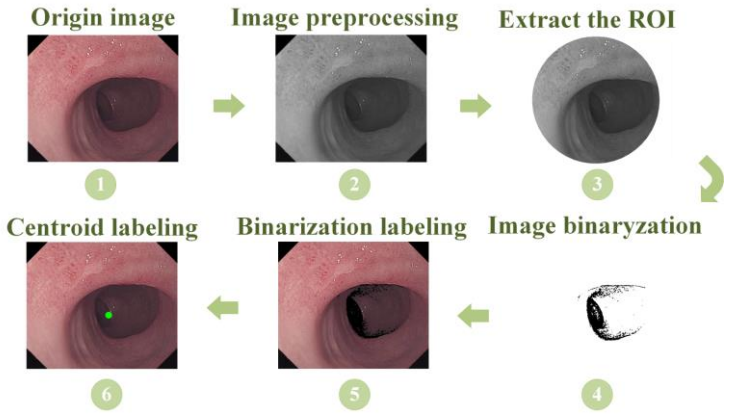

Figure 1. Endoscopic dark area method navigation process.

The dark area method developed in this study (see **Figure 1**) begins with performing a series of preprocessing steps on the image, including converting the image to grayscale format, applying a smoothing filter to reduce noise, and increasing the image contrast to highlight important features. Subsequently, the region of interest (ROI) is extracted at the center of a circle with the height of the image as its diameter, thereby enabling the processing to be focused on the part containing the most

important navigational information. This not only improves the computational efficiency of the process, but also effectively reduces the interference caused by light reflections in the edge region.

After that, the image is transformed into a binary image by applying a threshold (set to 35) where the dark area represents black pixel points. Navigation points (green-marked points) are derived by computing the centroid of these black pixel points, furnishing essential information for operating the endoscope.

In order to illustrate the computational process of the dark zone method more clearly, we introduce the following formula derivation. Suppose that the light intensity $I(x, y)$ of each pixel point in the image can be calculated by the following equation:

$$I\left(x, y\right) = I_0 \times \frac{1}{d\left(x, y\right)^2} \tag{2}$$

where $d(x, y)$ is the distance from the light source to the pixel point (x, y). By calculating the light intensity of each pixel point, the light intensity distribution of the whole image can be obtained. The image is then converted to a binary image by setting a threshold *T*, where dark areas represent black pixel points. The selection of the threshold *T* is determined experimentally as follows: (1) Number of experiments: A total of 30 experiments were conducted, with different colon models and different light source intensities selected for each experiment. (2) Data Acquisition: A high-resolution camera was used to acquire the image data, and 30 frames were acquired per second. (3) Data processing: The acquired image data were grayed out, smoothed and filtered, and contrast enhanced. Then the light intensity of each pixel point is calculated, and the area and location of dark areas under different thresholds are counted.

Through the above experiments, we determined the threshold value $T = 35$ as the best threshold value. The navigation point (green-marked point) is derived by calculating the center of these black pixel points, which provides important information for operating the endoscope.

2.2. Design of optical flow method

This previous subsection discusses the dark area method, which provides an important reference point for endoscopic navigation. However, relying solely on the dark area method as a reference may not be entirely reliable. For example, when the endoscope is close to the colonic wall, the image tends to be brighter due to the proximity of the light source to the colonic wall, resulting in the dark areas being less visible or even disappearing.

Therefore, we introduce the Lucas-Kanade [23] optical flow method to overcome the limitations of the dark area method. This method estimates the motion of pixel points as the endoscope traverses the colon. Analyzing a sequence of two consecutive frames of images captured by the endoscopic camera provides navigational hints. The optical flow can be expressed as

$$\frac{\partial I}{\partial x}u + \frac{\partial I}{\partial y}v + \frac{\partial I}{\partial t} = 0 \tag{3}$$

where $u = \frac{dx}{dt}, v = \frac{dy}{dt}$ denote the velocity vectors of the optical flow along the *X*-axis and *Y*-axis, respectively, and denote the partial derivatives of the grayscale of the pixel points in the image along the *X* and *Y*-axis, respectively. $\frac{\partial I}{\partial x}, \frac{\partial I}{\partial y}, \frac{\partial I}{\partial t}$ is obtained from the image data, and (u, v) is the vector of the requested optical flow.

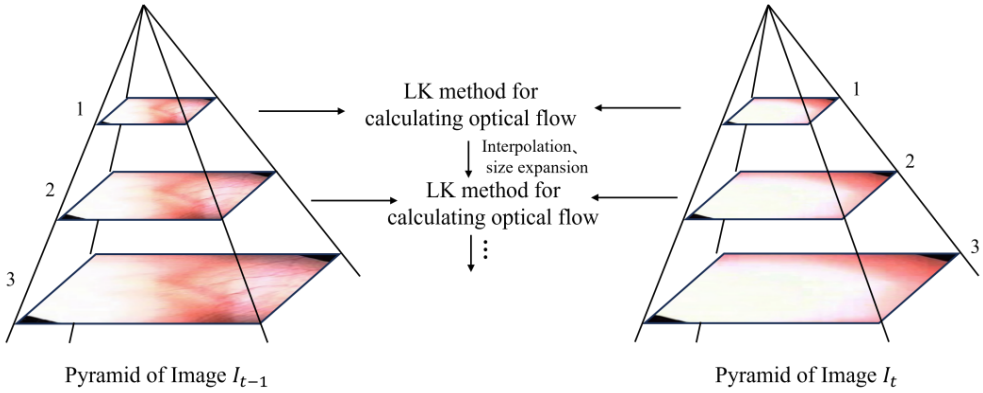

Figure 2. Pyramid structure of images.

In this study, a preprocessing step is performed on the image, including grayscale conversion, smoothing filtering, and contrast enhancement. Following these steps, a region of interest (ROI) is extracted to reduce the computational complexity, thereby enhancing computational efficiency. A three-level pyramid structure is established to progressively reduce the image resolution through downsampling, allowing for a focused examination of key features at each tier. The image pyramid structure constructed in this paper is shown in **Figure 2**. At each level of the pyramid, feature points are selected at intervals of every 5 pixels in both the vertical and horizontal directions. For each feature point, its optical flow is computed using the Lucas-Kanade algorithm with a window size of 5 × 5. In this process, the Lucas-Kanade algorithm is employed to determine the motion vectors of the feature points by calculating the image gradients between neighboring frames. These motion vectors are then utilized to infer the displacement direction and velocity of the feature points, which in turn generates the motion trajectories of the feature points.

In order to ensure the accuracy of the tracking, multiple iterations of feature points were performed for each pyramid level. Multi-scale information was used to optimize the results of feature point matching. Consequently, the trajectories of all feature points were delineated with blue lines, and the real-time movement of the endoscope was guided by identifying the center of mass of these blue trajectories (green-marked points). The process of calculating navigation points by the optical flow method is illustrated in **Figure 3**.

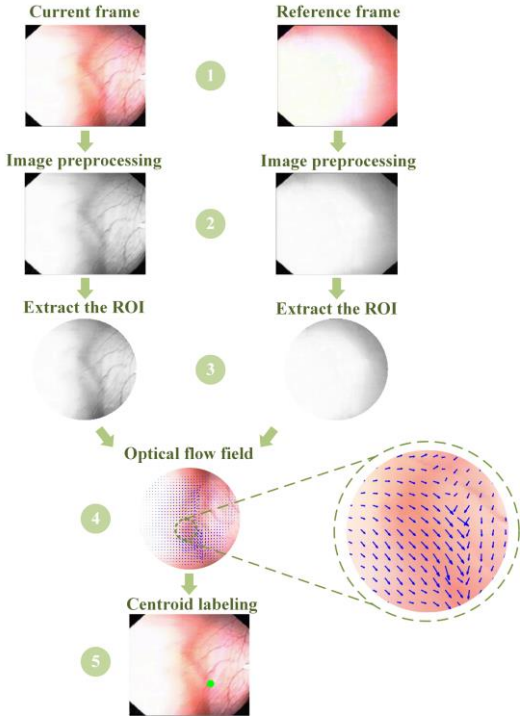

Figure 3. Endoscopic optical flow method navigation process.

3. Navigation strategies for colonic collapse and tumors

3.1. Detection and processing of colonic collapse

Colonic collapse may occur during endoscopic navigation, which can obstruct the smooth advancement of the endoscope and create challenges for our navigation method. Specifically, collapsed regions may lead to irregular dark areas in the image, which are not ideal for navigation, rendering the dark area method non-applicable. In addition, the lack of texture information in collapsed regions hinders the optical flow method, making it challenging to track feature points in the image. Consequently, it is crucial to distend the collapsed colon to restore the original configuration of the colon before applying the method described previously.

In cases where insufflation is not suitable, dilatation operations in morphology can be used to simulate the process of dilatation of the colon [24]. This is done by converting the image to a grayscale image and binarizing it and then enhancing the stenotic regions using an erosion operation. Stenotic regions are identified by calculating the aspect ratio of each connected region, and if the aspect ratio exceeds a threshold (set to 2), the region is considered to be stenotic. Once collapse is detected, a closure operation (dilation followed by erosion) is performed on the region to restore part of the colonic structure. The processed image can be navigated using either the dark area method or the optical flow method, the choice of which is described in Section 4.

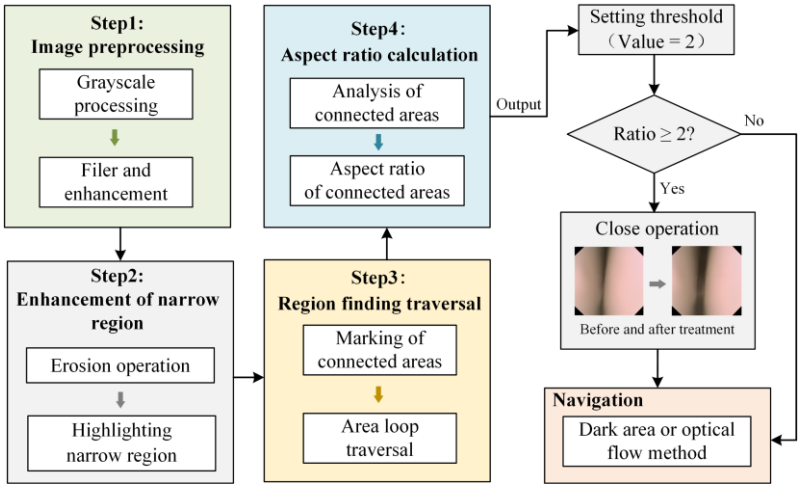

Figure 4. Schematic diagram of collapse detection and processing strategy.

Erosion and dilation operations are the primary methods. The strategy for identification and processing is shown in **Figure 4**. Initially, the image is converted to grayscale and binarized, after which the narrow regions are enhanced with an erosion operation. The erosion operation is used because it is applied to the white parts (highlights). Next, connected regions are labeled on the binarized image after erosion. The loop is utilized to traverse each connected region (in which there may be more than one connected region in the image), and the aspect ratio of each region is calculated. Here, the 'aspect ratio' refers to the ratio of the long and short axes of the region, that is to say, the ratio between the maximum and minimum width of the area. The aspect ratio can be expressed as

$$AspectRatio = \frac{MajorAxisLength}{MinorAxisLength} \tag{4}$$

where $MajorAxisLength$ represents the length of the main axis, which is usually the longest axis in the region, while $MinorAxisLength$ represents the length of the secondary axis, which is usually the shortest axis in the region.

If the aspect ratio exceeds a predetermined threshold (set to 2), it is identified as a narrow region. If there is at least one narrow region, it can be considered a colonic collapse. Once the region is detected as collapsed, a close operation (dilation followed by erosion) is performed in this region.

The collapsed images, processed through morphological operations, effectively restore part of the colonic structure. The endoscope can be guided forward, employing the dark area or optical flow method. The choice between the dark area method and the optical flow method is covered in Section 4.

3.2. Detection and segmentation of colonic tumor

Tumors pose a significant challenge during endoscopic procedures, often obstructing the field of view and impeding precise navigation. This obstruction poses difficulties to the system in locating the navigation point, hindering endoscopic exploration accurately. Direct contact with the tumor area must be avoided to prevent exacerbating tumor growth.

To address this challenge, we employ deep learning techniques for tumor detection and segmentation to avoid tumor regions effectively. The specific strategy (see **Figure 5**) is as follows: Endoscopic images undergo classification using a convolutional neural network [25] - and tumor regions are further segmented and eliminated at the pixel level by introducing semantic segmentation techniques. Subsequently, the endoscope can be guided forward, employing the dark area or optical flow method.

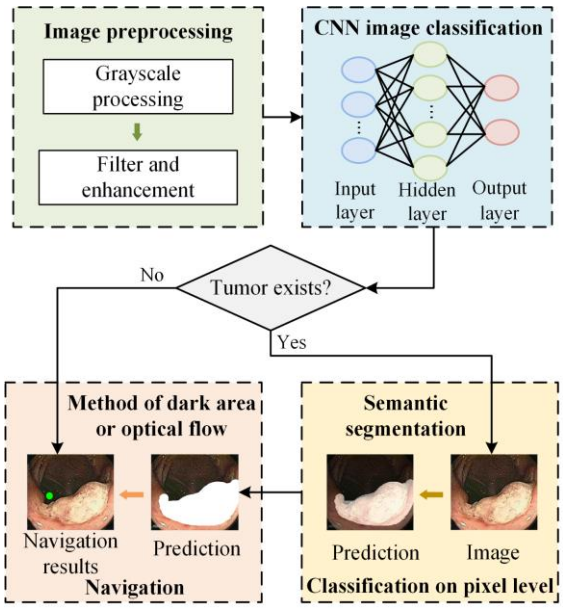

Figure 5. Schematic diagram of tumor detection and processing strategy.

Real-time image processing of tumors is critical during examination. In addition to ensuring high real-time performance, maintaining high accuracy is also vital. Therefore, striking a balance between accuracy and real-time performance is the key to achieving effective navigation.

3.2.1. Detection of colonic tumor

Considering network accuracy and real-time performance requirements, we compare three lightweight models: MobileNet-V2 [26], ShuffleNet [27], and EfficientNet-B0 [28]. These models demonstrate excellent accuracy while maintaining high computational efficiency. In addition, all three models employ a migration learning approach [29,30] that facilitates the adaptation of the models for specific classification tasks involving endoscopic images.

The data are from Gastrointestinalatlas.com and contain 1000 images with and without tumors. The dataset is split into 80% for training and 20% for testing and validation. Furthermore, data augmentation is performed, through four transformations (rotation, flipping, blurring and lighting changes) [31].

The experimental results are assessed using three main metrics: Accuracy, model parameter count, and average inference time. Inference time refers to the duration the neural network needs to process a frame. Each network model underwent testing on 50 tumor images to calculate the average reasoning time. **Table 1** summarizes the results.

Table 1. Results of evaluation of indicators in tumor detection.

Models	Accuracy/%	Params/M	Inference time/ms
MobileNet-V2	91.68	3.50	32
ShuffleNet	92.37	1.40	29
EfficientNet-B0	93.59	5.31	73

Table 1 shows that while EfficientNet-B0 exhibits superior accuracy compared to the other models, its inference time is longer than that of the other two models. MobileNet-V2 displays a lower level of accuracy. ShuffleNet balances accuracy and speed, making it the preferred tumor detection model for our system.

Training details: ShuffleNet is trained using a stochastic gradient descent (SGD) optimizer with an initial learning rate of 0.01, momentum of 0.9, and weight decay of 4×10^{-5}. The loss function is a cross-entropy loss function. During the training process, the learning rate decays linearly with the number of training steps. The total number of training steps is 300,000, and validation is performed once every 10,000 steps.

3.2.2. Segmentation of colonic tumor

Semantic segmentation analyzes tumor images, helping doctors differentiate tumors from nearby healthy tissues by classifying each pixel. It facilitates more accurate diagnosis and navigation planning.

For real-time requirements, the DeepLabV3+ model with encoder MobileNetV2 [32] is chosen. The model is tested on a tumor image dataset, which is also sourced from Gastrointestinalatlas.com. and is compared to the DeepLabV3+ [33] model with the ResNet50 encoder. The images are divided into 80% for training and 20% for testing and validation, following the data augmentation process described previously.

The experimental results are evaluated using three metrics: Mean intersection over union (MIoU), number of model parameters (Params), and average inference time. The average time for segmenting 50 images is also calculated. **Table 2** summarizes the results.

Table 2. Results of evaluation of indicators in tumor segmentation.

Models	MIoU/%	Params/M	Inference time/ms
DeeplabV3+ (ResNet50)	83.59	27.68	87
DeeplabV3+ (MobileNetV2)	81.80	5.99	54

As illustrated in **Table 2**, while the DeepLabV3+ (ResNet50) model exhibits a relatively high MIOU, its numerous parameters and prolonged inference times may present challenges for real-time endoscopic navigation systems. The MIOU of DeepLabV3+ (MobileNetV2) is marginally lower than that of DeepLabV3+ (ResNet50). However, the former is faster. Consequently, the DeepLabV3+ (MobileNetV2) model is well-suited to the purpose of providing the requisite accuracy and speed for endoscopic navigation systems.

Training details: DeepLabV3+ (MobileNetV2) is trained using a stochastic gradient descent (SGD) optimizer with an initial learning rate of 0.01, momentum of 0.9, and weight decay of 4×10^{-5}. The loss function is a cross-entropy loss function.

During the training process, the learning rate decays linearly with the number of training steps. The total number of training steps is 300,000, and validation is performed once every 10,000 steps.

Removing the identified tumor within the tumor region is imperative to ensure the navigation system's efficiency. Upon successful removal, the navigation system will determine the optimal approach (see Section 4), whether dark area or optical flow. Subsequently, this chosen method will be applied to the endoscopic image of the removed tumor to calculate the navigation point. Physicians will then track this point to minimize unnecessary contact and potential complications, ensuring the accuracy and safety of the navigation process.

3.2.3. Quantitative analysis of threshold selection

In order to improve the scientific validity of the methodology, we performed a quantitative analysis of the threshold selection. Specifically, we used sensitivity analysis to assess the reasonableness and reliability of the thresholds. Through the sensitivity analysis, we determined the effects of different thresholds on the model performance and thus selected the optimal thresholds. Sensitivity index: Obtained by calculating the derivatives or correlation statistics of the model output to the parameter change, the higher value indicates that the model is more sensitive to the parameter. According to the size of the sensitivity index, the sensitivity is categorized into three levels: High, medium, and low.

Hyperparameter tuning is a key step in the training of deep learning models, which directly affects the performance of the models (**Table 3**). The following is the specific procedure of our hyperparameter tuning for ShuffleNet and DeepLabV3+ models: (1) Learning rate: Learning rate is one of the most important hyperparameters in deep learning model training. The learning rate determines how much the gradient descent optimization algorithm moves in the parameter space. Too small a learning rate will lead to slow or even stagnant training; too large a learning rate will lead to unstable training dynamics. We choose an initial learning rate of 0.01 and use a linear decay strategy in the training process. (2) Batch size: The batch size determines the number of samples to be captured in each forward and back propagation. Smaller batch sizes will result in more noise but allow for more frequent parameter updates; larger batch sizes result in smaller variance in the gradient estimates of individual batches, which helps the network to train more stably, but this may also make the training process require more computational resources and time. We choose a batch size of 32. (3) Weight decay coefficient: Weight decay can limit the magnitude of parameter variation and play a regularizing role. We choose a weight decay coefficient of 4×10^{-5}. (4) Optimizer: We choose a stochastic gradient descent (SGD) optimizer with a momentum of 0.9. The momentum parameter is used to speed up the training and help avoid falling into local optima. (5) Learning rate decay strategy: Learning rate decay refers to gradually decreasing the learning rate of the model as the number of training iterations increases. We use a linear decay strategy to gradually reduce the learning rate as the number of training steps increases.

Table 3. Sensitivity analysis data.

Parameter name	Original value	Range of change	Sensitivity index	Sensitivity description
Learning rate	0.01	0.001~0.1	0.85	High
Batch size	32	16~64	0.45	Medium
Weight decay	4×10^{-5}	1×10^{-6}~1×10^{-4}	0.30	Low

4. Adaptive navigation strategy

4.1. Overview of the strategy

We have developed an adaptive navigation strategy (see **Figure 6**) rooted in a thorough analysis of image characteristics to fully harness the advantages of the dark area method and the optical flow method in diverse environments. Initially, the system identifies and addresses specific circumstances. Following the preprocessing of the image, the system detects the presence of collapse. Upon detection, the system extends the collapsed region and subsequently assesses the presence of tumors within the image. Precise tumor segmentation and removal operations are conducted in cases where tumors are detected. Subsequently, the system extracts and binarizes the image's ROI.

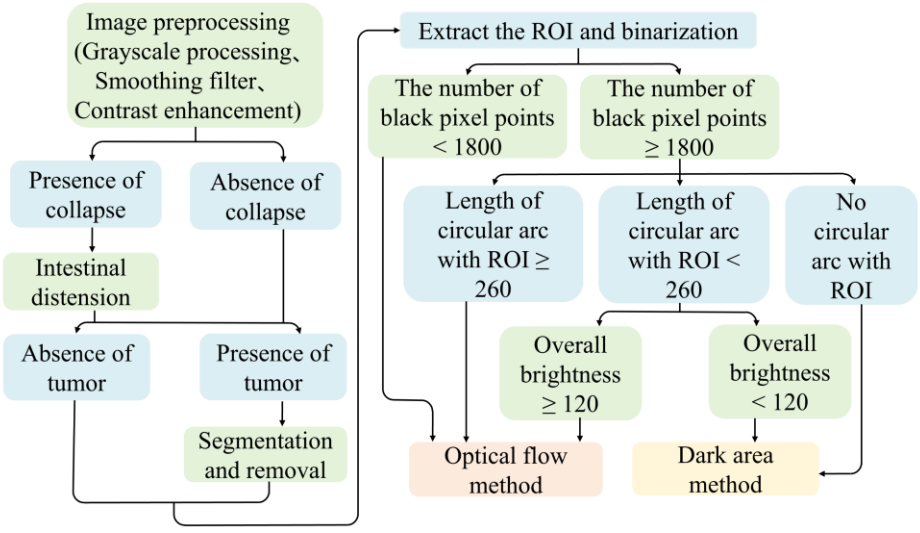

Figure 6. Schematic diagram of navigation method fusion strategy.

Then, a thorough analysis is conducted to determine the optimal navigation method. The navigation point is calculated by the system under the optimal navigation method, and the operator can then utilize the endoscope in accordance with the navigation point.

The specific classification process, which involves classifying an image and selecting a navigation method based on features such as the number of black pixel points, the length of the arc, and overall brightness, is described in detail in Section 4.2: Ordinary case analysis in navigation.

4.2. Ordinary case analysis in navigation

The analysis focused on three key features: The number of black pixel points after the binarization of the image, the length of the arc formed between the dark area and the ROI, and the overall brightness of the image. The number of black pixel points is correlated with the significance of the dark area in the image, serving as a metric to assess both the extent and importance of this region. The length of the arc reflects the distance between the endoscope and the colonic wall to a certain degree, which is quantified by the number of points along the arc. The overall brightness is measured by calculating the brightness histogram of the image.

Figure 7 illustrates four ordinary cases in the colon (without collapse and tumor). The original images of the four cases are displayed in **Figure 7a1–d1**. The results after binarization of the four cases are shown in **Figure 7a2–d2**. The brightness histograms of the four cases are shown in **Figure 7a3–d3**.

In Case 1, the binarized image contains a high number of black pixel points but no circular arc with the ROI (**Figure 7a2**). In Case 2, the binarized image shows a high number of black pixel points, a short circular arc with the ROI (**Figure 7b2**), and low brightness (**Figure 7b3**). In Case 3, the binarized image has a high number of black pixel points and forms a long circular arc with the ROI (see **Figure 7c2**). In Case 4, the binarized image contains no black pixel points (see **Figure 7d2**) and has high brightness (see **Figure 7d3**).

The process of determining the method of navigation in the four cases in **Figure 7** is described in detail in conjunction with the classification process in **Figure 6**. First, the image is pre-processed, including grayscale conversion, smoothing filters, and contrast enhancement. The image is then binarized as in **Figure 7a2–d2**. At this point, the number of black pixel points in the binarized image is initially considered. This reflects the distinctiveness of the dark area characteristics in the image.

A threshold of 1 (value is 1800) is established. When the number of black pixel points after binarization falls below threshold 1, indicating that the brightness of the image is relatively high overall. At this point, the endoscope is close to the colonic wall. Here, the optical flow method is employed for navigation. In Case 4, it is evident that no black pixel points are formed, as illustrated in **Figure 7d2**. The image brightness for this case is markedly high (as evidenced by **Figure 7d3**), which is navigated using the optical flow method.

However, when the number of black pixel points exceeds or is equal to threshold 1 after binarization, it signifies the prominent presence of the dark area characteristics within the image. In Case 1–Case 3, a distinct dark area is observed, as illustrated in **Figure 7a2–c2**. At this juncture, the arc formed between the dark area and the ROI is analyzed.

In Case 1, there is no circular arc between the dark area and the ROI, as shown in **Figure 7a2**. It implies that the dark area region is close to the image's center. This scenario arises when there is no noticeable curvature in the field of view of the endoscope. In this case, the dark area method is deemed for navigation.

If the dark area forms an arc with the ROI, the length of the circular arc formed between the dark area and the ROI is evaluated, and the threshold 2 (value is 260) is set. In Case 3, the circular arc length is greater than or equal to the threshold 2, as

shown in **Figure 7c2**. It infers that the distance between the endoscope and the colonic wall is close. In such instances, the optical flow method is more effective in utilizing local dynamic information to provide accurate navigation information. Conversely, the dark area method is no longer applicable due to limitations in the field of view and image occlusion.

In Case 2, the circular arc length is less than threshold 2, as shown in **Figure 7b2**. It suggests a distance between the endoscope and the colonic wall. However, relying solely on this criterion does not determine whether to employ the dark area or optical flow methods. In such scenarios, additional judgment is conducted based on the image's brightness. A threshold of 3 (value is 120) is established. In Case 2, the overall brightness of the image is greater than or equal to threshold 3, as shown in **Figure 7b3**. It infers that the endoscope is in a curved area of the colon with greater curvature, closer to the colonic wall. The optical flow methods can provide more precise navigation information.

However, if the overall brightness of the image is less than threshold 3, it signifies a more significant presence of the dark area characteristics in the image. In such a case, the endoscope is situated in the straight or less curved colonic region, warranting utilization of the dark area method.

The navigation points are labeled with green points in **Figure 7a4–d4** accordingly.

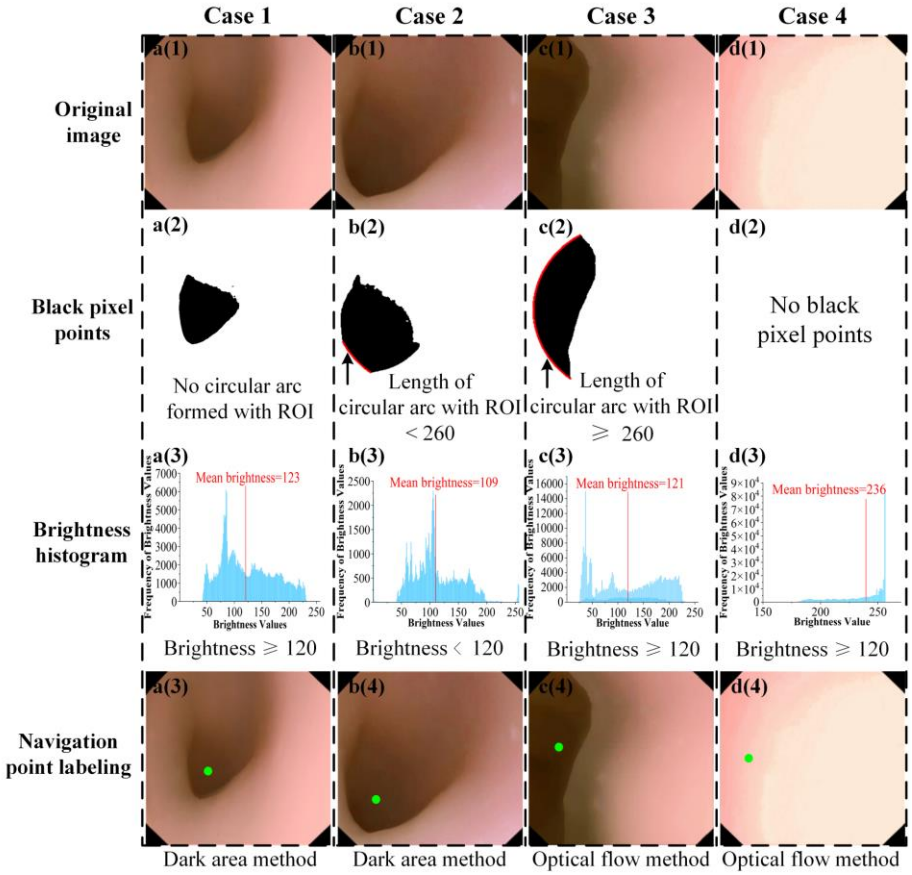

Figure 7. Schematic diagram of the four ordinary cases: **(a1–d1)** original images of the four cases; **(a2–d2)** black pixel points in four cases; **(a3–d3)** brightness histogram of the four cases; **(a4–d4)** navigation point labeling in four cases.

The thresholds 1, 2, and 3 are determined through a series of experiments. The endoscopes' resolution is 1280 × 720, a standard resolution for medical endoscopes. Data is collected and analyzed from endoscopes across various colonic regions, focusing on factors such as the number of black pixel points after binarization, the length of the circular arc formed by the ROI and the dark area, and the overall brightness.

By performing a multifactorial navigation bias analysis (**Table 4**), it was found that navigation bias increased by 37% (due to feature occlusion) for tumor diameters >2 cm, and that for every 1 kPa increase in intestinal wall stiffness (as quantified by biomechanical modeling), the optical flow method error rose by 22%.

Table 4. Multifactor navigation deviation analysis.

Influencing factors		Range of deviation (mm)	Significance (*P* value)	Clinical relevance
Bowel site	Ascending colon	0.81 ± 0.29	0.126	Large anatomical curvature and artifacts
	Descending colon	1.20 ± 0.53	0.030	Thick intestinal wall musculature, lagging optical flow tracking
Lesion type	Tumor (≥ 2 cm diameter)	2.11 ± 0.70	0.008	Higher rate of feature point loss due to occlusion
	Inflammatory stenosis	1.52 ± 0.58	0.021	Mucosal edema reduces image contrast

4.3. Special case analysis in navigation

When the system detects a special situation (collapse or tumor), take appropriate measures, including dilation of the collapsed colon and removal of the tumor. The following steps are the same as in the ordinary cases above, namely, the number of black pixel points after binarization, the length of the circular arc formed between the dark area and the ROI, and the overall brightness of the image are analyzed in sequence to determine whether the optical flow method or the dark area method is employed.

Four specific cases involving tumors or collapses are chosen for analysis (see **Figure 8**). The original images of these cases are depicted in **Figure 8a1–d1**, and it is observed that both images in **Figure 8a1** and **Figure 8b1** exhibit a collapsed colon. Following the distension of the collapsed colon, the colonic structure is restored to a certain extent, as shown in **Figure 8a2,b2**. In contrast, tumors of varying sizes are evident in **Figure 8c1,d1**. These tumors are segmented and removed, resulting in **Figure 8c2,d2** Subsequent analysis of **Figure 8(a2–d2)** is then conducted sequentially using the comprehensive judgment method established previously. The results after binarization of the four cases are shown in **Figure 8a3–d3**. The brightness histograms of the four cases are shown in **Figure 8a4–d4**.

The process of determining the method of navigation in the four cases in **Figure 8** is described in detail in conjunction with the classification process in **Figure 6**. Since the choice of navigation methods in the ordinary case has already been described in detail, only the choice of methods is briefly analyzed here.

In Case 5, the image is binarized, yielding many black pixel points. However, a short circular arc is formed with the ROI (see **Figure 8a3**), and the overall brightness is high (see **Figure 8a4**). The optical flow method is chosen for navigation.

In Case 6, the binarized image displays many black pixel points and forms a long circular arc with the ROI (see **Figure 8b3**). Navigation is also done using the optical flow method.

In Case 7, the number of black pixel points also remains high, and a long circular arc is formed with the ROI (see **Figure 8c3**); the optical flow method is used.

In Case 8, the binarized image contains a high number of black pixel points but fails to form a circular arc with the ROI (see **Figure 8d3**), leading to the selection of the dark area method.

Figure 8a5–d5 shows four cases of navigation points computed by the optical flow method or the dark area method, labeled on the original image.

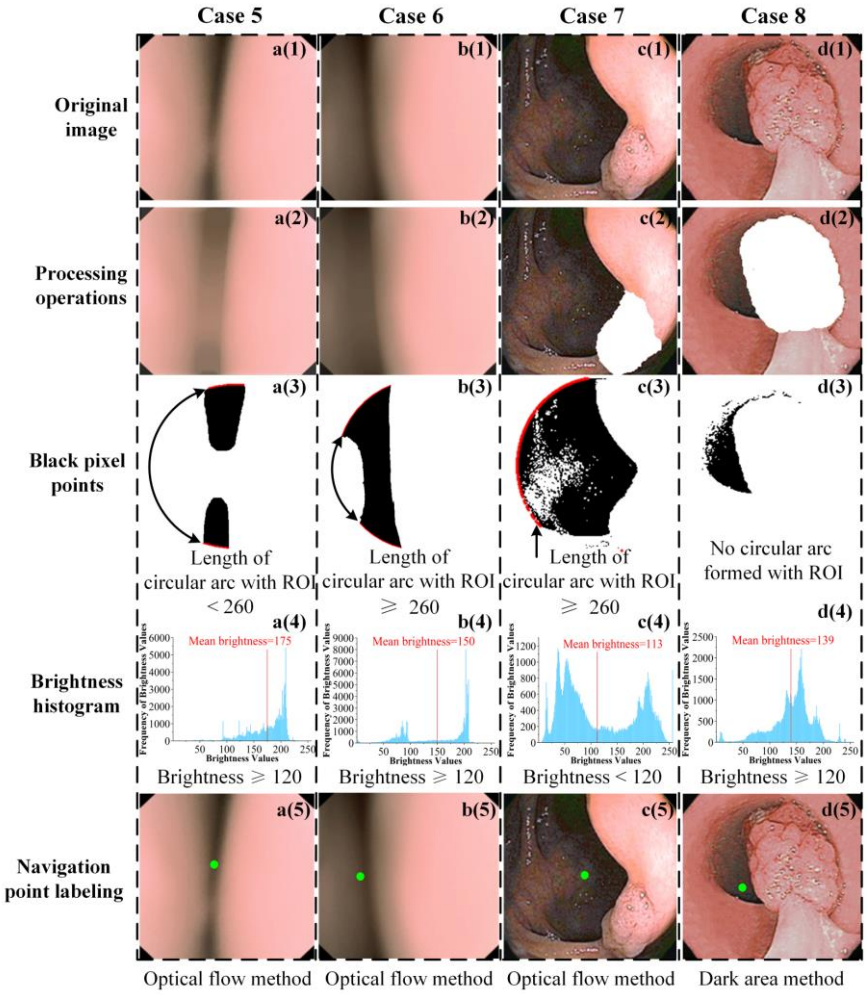

Figure 8. Schematic diagram of the four special cases: **(a1–d1)** original images of the four cases; **(a2–d2)** processing operations of the four cases; **(a3–d3)** black pixel points in four cases; **(a4–d4)** brightness histogram of the four cases; **(a5–54)** navigation point labeling in four cases.

5. Experimental validation

5.1. Experiment setup

An experimental setup, illustrated in **Figure 9a**, comprises three main components: A computer, an endoscope, and a simulated colon model. A computer is

used to execute our navigation system. The endoscope features a four-way adjustment capability, enabling it to simulate the manipulations performed by physicians. The endoscope is connected to a computer and the human-computer interface (see **Figure 9b**) on the computer displays the endoscope's real-time captured images. The interface captures images instantly for analysis and displays navigation points. In this interface, a circle is formed around the visual center (the radius is 20% of the screen vision). When the calculated navigation point (green marked point) is located outside the circle, the endoscope needs to be oriented according to the position of the navigation point in relation to the visual center. As shown in **Figure 9c**, the endoscope will be controlled to bend in the direction of the lower-right corner to approach the center of vision.

The simulated colon model utilized in this study is not only used to validate the performance of the endoscopic navigation system but also serves as a tool for pre-service training of endoscopists to enhance their operating skills.

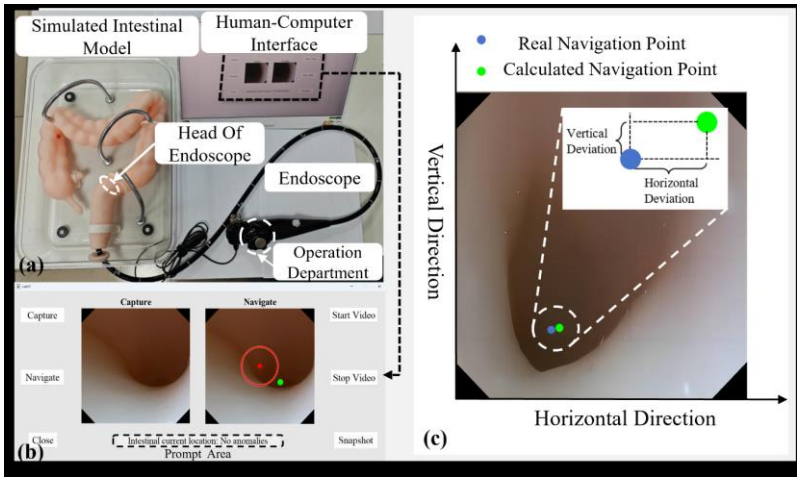

Figure 9. The experiment of endoscopic navigation: **(a)** experimental setup diagram; **(b)** human-computer interface diagram; **(c)** simulated colon model diagram.

In the experiment, the endoscope traverses through the simulated colon while the navigation system calculates navigation points in real-time. **Figure 10** shows six different moments in endoscopic navigation, as shown in **Figure 10a–f**. Each image (see **Figure 10a–f**) shows the current position of the endoscopic lens and the corresponding real points to navigate. The real navigation points were obtained by averaging the navigation points manually labeled by five experienced testers on the recorded experimental videos. Each individual performed three separate markings and received prior uniform training. The horizontal and vertical distances between the calculated navigation point and the real navigation point are regarded as horizontal deviation and vertical deviation (see **Figure 9c**).

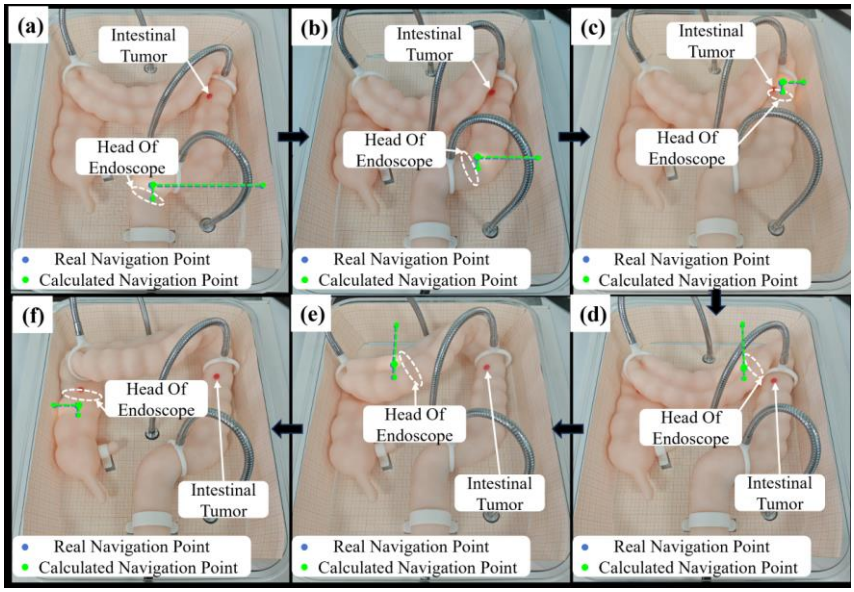

Figure 10. Process of endoscopic navigation: **(a–f)** six different moments in endoscopic navigation.

5.2. Evaluation of basic performance indicators

5.2.1. Navigation accuracy

Deviations (see **Figure 9c**) in the horizontal and vertical directions are measured between the calculated and real navigation points to evaluate the accuracy of the system. The processed image had a resolution of 720 × 720, and the final displayed image size is 82 × 82 m. Each pixel is calculated to be 0.114 mm in the display area, allowing for mapping of pixel-level differences in the image to physical space.

Figure 11 presents three groups of horizontal and vertical deviations of the system. The total time required for each experiment varies due to differences in the speed of advancement of each endoscope. The overall average horizontal deviation of the system is 3.15 mm, and the overall average vertical deviation is 2.51 mm. The optical flow method is employed on three occasions throughout each experiment. These instances occur in the curved segment of the sigmoid colon, the curved segment at the junction of the descending and transverse colon, and the curved segment at the junction of the transverse and ascending colon. It can be observed that the deviation of the dark area method is lower than that of the optical flow method, with the exception of the second dark area method. This is due to the fact that the optical flow method is susceptible to changes in image dynamics. In the second segment of the colon using the dark area method, the deviation of the dark area method increases due to the presence of the tumor. The combination of the dark area method and the optical flow method completes the navigation of the entire colon.

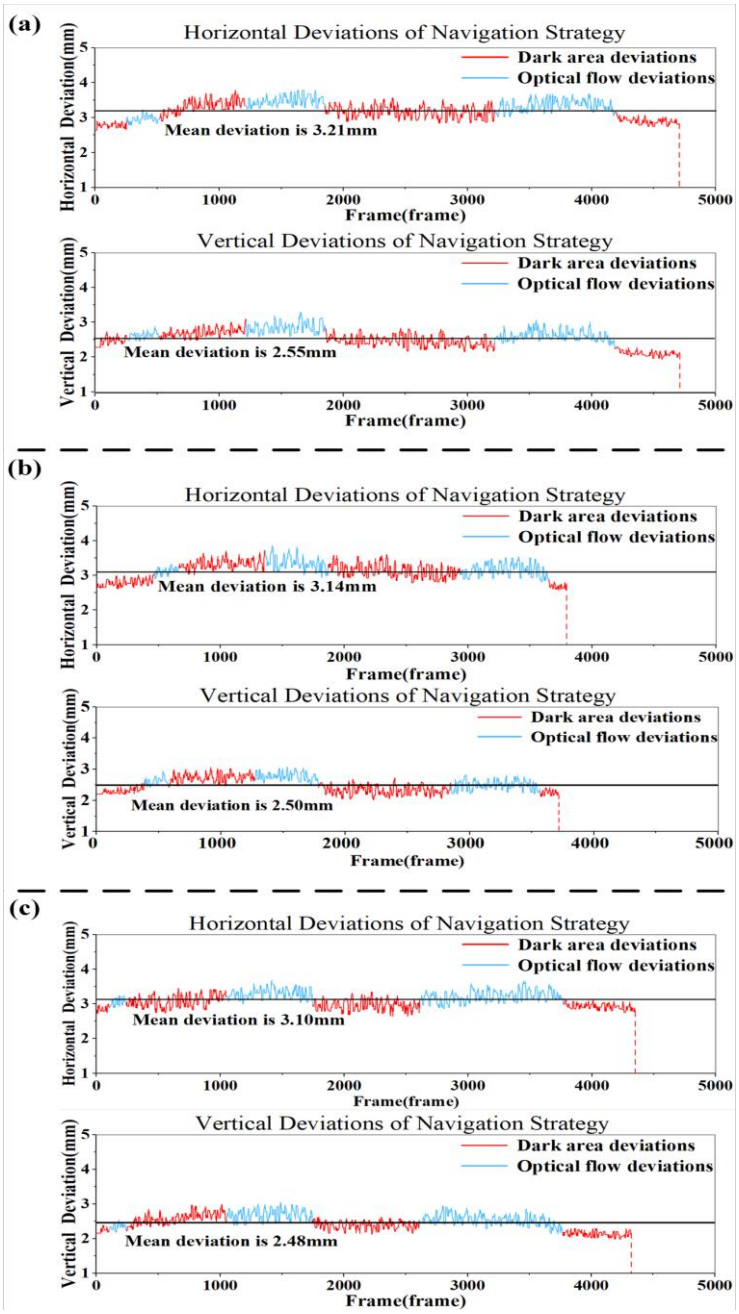

Figure 11. Endoscopic navigation deviations: **(a)** horizontal deviation and vertical deviation of the first group; **(b)** horizontal deviation and vertical deviation of the second group; **(c)** horizontal deviation and vertical deviation of the third group.

5.2.2. Navigation success rate

The following two scenarios are selected to evaluate the navigation success rate. One is tested in the colon with different degrees of curvature. Four colon segments with different levels of curvature (straight, mild, moderate, and severe) are chosen for testing. Mild curvature typically ranges from 15° to 45°, while moderate curvature occurs at angles between 45° and 90°. Severe curvature is classified as an angle over 90°.Three segments of the straight and one segment of each of the other curved segments of the colon are selected, totaling six segments. These segments of the colon are free of special conditions such as tumors and collapses, maintaining good lighting

conditions. Each segment of the colon is conducted when experiments are performed 20 times. The navigation success rate is 100% for straight and mildly curved colon, indicating that the system can navigate effectively under these conditions. The success rate is 95% for moderate curvature of the colon; however, it decreases to 75% in the presence of severe curvature of the colon. This decline can be attributed to the challenges the endoscopic camera encounters in capturing the comprehensive field of view within the highly curved colon. Such curvature hampers image processing and feature recognition accuracy, thereby impacting navigation accuracy.

The other is tested in the colon with special conditions. Experiments are conducted on the colon model with unique conditions: One with a tumor and another with a collapse. Both segments are relatively straight and have adequate lighting. Twenty tests are conducted in each segment, and the navigation success rate for the tumor-containing colon is 90%. Despite the relatively high success, an analysis of the failures reveals that the presence of the tumor leads to localized areas of narrowing, increasing the difficulty of endoscopic navigation. This is the reason for the navigation failure. The success rate for a collapsed colon is 80%. It is important to note that the distension process may not be able to accurately restore the original shape of the colon, especially in the case of non-uniform collapse. This leads to a bias in the computation of the navigation points.

Considering all test scenarios, the overall success rate of our endoscopic navigation system is 92.5%. The success rate is reduced in specific circumstances, such as a high degree of curvature or the presence of collapse, but the overall performance remains satisfactory.

5.2.3. Navigation in real time

The processing time per frame is evaluated using two methods. The dark area method is capable of processing each frame in a mere 9 ms, while the optical flow method requires 278 ms per frame. The time from frame capture to updating navigation points is also measured. In normal conditions, the dark area method takes 24 ms, compared to 302 ms for the optical flow method. With the tumor, the dark area takes 365 ms and optical flow takes 727 ms. For the collapsed region, the dark area method takes 79 ms, and the optical flow method takes 354 ms. Overall, the real-time performance is satisfactory.

5.3. System evaluation

In order to assess the usefulness and general applicability of the system in greater depth, senior doctors and untrained laypeople were invited to participate in the system evaluation.

5.3.1. Doctor’s feedback

An evaluation of the endoscopic navigation system was conducted by an expert in endoscopy from the First Hospital of Shanxi Medical University. This expert has accumulated a wealth of clinical experience in the domain of colonoscopy and has been involved in related endoscopic technology research.

The expert provided feedback on the navigation system, stating that it provides clear and reliable guidance during real-time operation, thus facilitating the endoscopic insertion operation. Furthermore, the system is a valuable study as it reduces the

physical and mental exertion of the doctor during prolonged operations, thus improving the overall efficiency of the examination.

It is anticipated that, under the guidance of this expert, the navigation system will continue to be optimized, with a view to promoting its clinical application in the future.

5.3.2. Model usefulness and general applicability testing

In addition to providing further validation of the system's usefulness and general applicability, five laypeople were invited to test the navigation system using the simulated model. Each participant was required to complete the navigation task on the simulated colon model.

Prior to the test, participants were not provided with any training on endoscopic operation. Instead, they were merely shown a brief demonstration video of the operation before commencing the test. Each participant was required to utilize the navigation system to complete a comprehensive traversal task through the simulated colon model, with the system providing real-time prompts for navigation points. The participants' error frequency, and their feelings and feedback on the operation of the system were focused on.

The total failure counts for the five participants during their first three attempts were 4, 5, 3, 6, and 4, respectively (adjustments continued after each failure until the end of the colon model was reached). As their familiarity with the system increased, the number of errors gradually decreased. After three operations, all participants were able to successfully complete the navigation task with the assistance of the navigation system's prompts.

It is of greater significance that all participants affirmed the simplicity and intelligibility of the system's user interface, as well as the efficacy of real-time feedback during navigation in facilitating comprehension of operational requirements and enhancing controllability of the operation. The overwhelming majority of participants affirmed the efficacy of the navigation system in simplifying endoscopic operations, particularly for those with limited experience in this domain.

The results demonstrate that the navigation system is intuitive and accessible, even to operators without prior experience, enabling them to rapidly acquire the necessary skills and successfully complete complex navigation tasks. Consequently, the reliance on operational experience and protracted training is reduced.

5.4. Integration of experimental technical indicators with clinical diagnostic and therapeutic effects

To illustrate the positive impact of the navigation system on improving clinical diagnostic accuracy and reducing complications, we combined the experimental indicators with the clinical diagnostic results (**Table 5)**. The advantages of the navigation system in practical application were demonstrated through data comparison or case analysis. We chose a specific case for analysis. The diagnostic accuracy increased from 85% to 95%, and the complication rate decreased from 15% to 5% after using the adaptive method. This demonstrates the significant advantages of adaptive navigation systems in improving diagnostic accuracy and reducing complications. The correlation between bias and efficacy is shown in **Table 6**.

Table 5. Clinical end-use validation.

Navigation method	Diagnostic accuracy (%)	Complication rate (%)
Traditional method	85.13	15.37
Adaptive methods	95.26	5.09

Table 6. Deviation-efficacy correlation matrix.

Source of bias	Diagnostic sensitivity (*r*-value)	Operating time (*r*-value)	Risk of complications (*OR*-value)
Optical flow tracking lag	−0.63	0.51	1.821 (1.220–2.813)
Tumor segmentation residual	−0.71	0.67	2.152 (1.421–3.307)
Collapse artifact interference	−0.45	0.39	1.656 (1.112–2.503)

6. Discussion

This paper presents an intelligent system for navigating an endoscope in a complex intestinal environment. The system employs an adaptive pathfinding strategy that incorporates the dark area method and the optical flow method, aiming to improve the navigation performance. The system achieves a 92.5% success rate in a simulated intestinal model with an average horizontal deviation of 3.15 mm and an average vertical deviation of 2.51 mm, demonstrating high accuracy and reliability.

In contrast to the navigation method proposed by Hao et al., which only considered the presence of a dark area, our strategy combines the discriminative mechanisms of the three key factors and intelligently selects the most appropriate navigation method, thus improving the navigation accuracy in complex intestinal environments. In addition, our system includes specialized handling strategies for special cases such as colonic collapse and tumors, which have not yet been fully addressed in the study by Reilink et al.

However, a limitation of this study lies in the fact that only a limited range of intestinal curvature was tested. Further exploration and optimization of the system's performance in more complex curvature cases are imperative and will be a primary focus of future studies. Furthermore, the subsequent focus should be on extending the system to clinical applications.

7. Conclusion

We propose an adaptive strategy for intelligent colon endoscopic navigation in complex colonic environments. This system intelligently selects the most suitable navigation method by introducing a comprehensive discriminative mechanism, improving the adaptability to complex colonic environments. Moreover, specific processing strategies are designed for exceptional cases such as colonic collapses and tumors; the ability to respond to these special situations is further enhanced. The experimental results demonstrate that our system is capable of providing crucial information for endoscopic navigation, thereby enabling more precise and effective guidance of the endoscope through complex colonic environments. Furthermore, the system is straightforward to operate, allowing even inexperienced operators to quickly master and successfully perform endoscopic operations, thereby proving that our system can reduce the reliance on operating experience.

In terms of navigation accuracy assessment, we not only provided the average deviation but also analyzed the navigation deviation from multiple dimensions, which provided the direction for further optimization of the system, especially when dealing with complex anatomical structures and lesions, which requires further improvement of the navigation algorithm to enhance the accuracy. Meanwhile, we quantitatively analyzed the threshold selection, which provided a scientific basis for threshold selection and ensured that the model was balanced between high sensitivity and high specificity. In addition, we combined the experimental technical indicators with the clinical diagnosis and treatment effects and illustrated the positive impact of the navigation system on improving the accuracy of clinical diagnosis and reducing complications through data comparison and case analysis.

In summary, our adaptive navigation system performs well in complex colonic environments, not only improves navigation accuracy, but also reduces the dependence on operating experience, comprehensively evaluates the performance of the navigation system, and provides a scientific basis for further optimization of the system.

Author contributions: Conceptualization, XM and JG; methodology, XM and JG; software, XM; validation, XM, HH and JZ; formal analysis, XM and CL; resources, JZ; data curation, CL; writing—original draft preparation, XM; writing—review and editing, XM and JG; visualization, XM; supervision, GY; project administration, JG; funding acquisition, JG. All authors have read and agreed to the published version of the manuscript.

Funding: This research was funded by the National Natural Science Foundation of China, grant number 52275038 and 61803347.This research was funded by the Shanxi Province Science Foundation, grant number 202303021222087.

Ethical approval: Not applicable.

Data availability statement: The original contributions presented in this study are included in the article. Further inquiries can be directed to the corresponding author.

Conflict of interest: The authors declare no conflict of interest.

References

1. Bray F, Laversanne M, Weiderpass E, et al. The ever-increasing importance of cancer as a leading cause of premature death worldwide. Cancer. 2021; 127(16): 3029-3030. doi: 10.1002/cncr.33587
2. Bray F, Laversanne M, Sung H, et al. Global cancer statistics 2022: GLOBOCAN estimates of incidence and mortality worldwide for 36 cancers in 185 countries. CA: A Cancer Journal for Clinicians. 2024; 74(3): 229-263. doi: 10.3322/caac.21834
3. Li M, Wang B, Yang J, et al. Multistage adaptive control strategy based on image contour data for autonomous endoscope navigation. Computers in Biology and Medicine. 2022; 149: 105946. doi: 10.1016/j.compbiomed.2022.105946
4. Tang Y, Anandasabapathy S, Richards-Kortum R. Advances in optical gastrointestinal endoscopy: a technical review. Molecular Oncology. 2020; 15(10): 2580-2599. doi: 10.1002/1878-0261.12792
5. Siegel RL, Miller KD, Fuchs HE, et al. Cancer statistics, 2022. CA: A Cancer Journal for Clinicians. 2022; 72(1): 7-33. doi: 10.3322/caac.21708
6. Keswani RN, Crockett SD, Calderwood AH. AGA Clinical Practice Update on Strategies to Improve Quality of Screening and Surveillance Colonoscopy: Expert Review. Gastroenterology. 2021; 161(2): 701-711. doi: 10.1053/j.gastro.2021.05.041

7. Boini A, Acciuffi S, Croner R, et al. Scoping review: autonomous endoscopic navigation. Artificial Intelligence Surgery. 2023; 3(4): 233-248. doi: 10.20517/ais.2023.36
8. Gastone C, Skonieczna-Żydecka K, Marlicz W, et al. Frontiers of Robotic Colonoscopy: A Comprehensive Review of Robotic Colonoscopes and Technologies. Journal of Clinical Medicine. 2020; 9(6): 1648. doi: 10.3390/jcm9061648
9. Luo X, Mori K, Peters TM. Advanced Endoscopic Navigation: Surgical Big Data, Methodology, and Applications. Annual Review of Biomedical Engineering. 2018; 20(1): 221-251. doi: 10.1146/annurev-bioeng-062117-120917
10. Cagiltay NE, Ozcelik E, Berker M, et al. The Underlying Reasons of the Navigation Control Effect on Performance in a Virtual Reality Endoscopic Surgery Training Simulator. International Journal of Human–Computer Interaction. 2018; 35(15): 1396-1403. doi: 10.1080/10447318.2018.1533151
11. Prendergast JM, Formosa GA, Heckman CR, et al. Autonomous Localization, Navigation and Haustral Fold Detection for Robotic Endoscopy. Proceedings of the 2018 IEEE/RSJ International Conference on Intelligent Robots and Systems (IROS); 2018. doi: 10.1109/iros.2018.8594106
12. Reilink R, Stramigioli S, Misra S. Image-based flexible endoscope steering. Proceedings of the 2010 IEEE/RSJ International Conference on Intelligent Robots and Systems. Published online October 2010: 2339-2344. doi: 10.1109/iros.2010.5652248
13. Xia S, Krishnan SM, Tjoa MP, Goh PMY. A novel methodology for extracting colon's lumen from colonoscopic images. Systemics Cybern. Inform; 202.
14. Zhang Z, Qian J, Zhang Y, et al. An Intelligent Endoscopic Navigation System. Proc. Int. Conf. Mechatronics Autom; 2006. doi: 10.1109/icma.2006.257444
15. Liu Q, Li H, He L. Optical Flow Algorithm Based on the Medical Flexible Endoscope System. Electronic Sci. & Tech; 2015.
16. van der Stap N, Reilink R, Misra S, et al. The use of the focus of expansion for automated steering of flexible endoscopes. Proceedings of the 2012 4th IEEE RAS & EMBS International Conference on Biomedical Robotics and Biomechatronics (BioRob); 2012. doi: 10.1109/biorob.2012.6290804
17. Ciuti G, Visentini-Scarzanella M, Dore A, et al. Intra-operative monocular 3D reconstruction for image-guided navigation in active locomotion capsule endoscopy. Proceedings of the 2012 4th IEEE RAS & EMBS International Conference on Biomedical Robotics and Biomechatronics (BioRob); 2012. doi: 10.1109/biorob.2012.6290771
18. Abu-Kheil Y, Ciuti G, Mura M, et al. Vision and inertial-based image mapping for capsule endoscopy. Proceedings of the 2015 International Conference on Information and Communication Technology Research (ICTRC); 2015. doi: 10.1109/ictrc.2015.7156427
19. Floor PA, Farup I, Pedersen M. 3D reconstruction of the human colon from capsule endoscope video. Proc. Colour Vis. Comput. Symp. (CVCS); 2022.
20. Onogi S, Nakajima Y. Assessment of All-in-focus Image Quality in Shape-from-focus Technique. Sensors and Materials. 2023; 35(4): 1327. doi: 10.18494/sam4219
21. Jiang W, Zhou Y, Wang C, et al. Navigation strategy for robotic soft endoscope intervention. The International Journal of Medical Robotics and Computer Assisted Surgery. 2019; 16(2). doi: 10.1002/rcs.2056
22. Krishnan SM, Tan CS, Chan KL. Closed-boundary extraction of large intestinal lumen. Proceedings of 16th Annual International Conference of the IEEE Engineering in Medicine and Biology Society; 1994. doi: 10.1109/iembs.1994.411878
23. Lucas BD, Kanade T. An iterative image registration technique with an application to stereo vision. Proc. Int. Joint Conf. Artif. Intell; 1981.
24. Mondal R, Dey MS, Chanda B. Image Restoration by Learning Morphological Opening-Closing Network. Mathematical Morphology—Theory and Applications. 2020; 4(1): 87-107. doi: 10.1515/mathm-2020-0103
25. Albawi S, Mohammed TA, Al-Zawi S. Understanding of a convolutional neural network. Proceedings of the 2017 International Conference on Engineering and Technology (ICET); 2017. doi: 10.1109/icengtechnol.2017.8308186
26. Sandler M, Howard A, Zhu M, et al. MobileNetV2: Inverted Residuals and Linear Bottlenecks. Proceedings of the 2018 IEEE/CVF Conference on Computer Vision and Pattern Recognition; 2018. doi: 10.1109/cvpr.2018.00474
27. Zhang X, Zhou X, Lin M, et al. ShuffleNet: An Extremely Efficient Convolutional Neural Network for Mobile Devices. Proceedings of the 2018 IEEE/CVF Conference on Computer Vision and Pattern Recognition; 2018. doi: 10.1109/cvpr.2018.00716
28. Tan M, Le Q. Efficientnet: Rethinking model scaling for convolutional neural networks. Proc. Int. Conf. Mach. Learn; 2019.
29. Pan SJ, Yang Q. A Survey on Transfer Learning. IEEE Transactions on Knowledge and Data Engineering. 2010; 22(10): 1345-1359. doi: 10.1109/tkde.2009.191

30. Weiss K, Khoshgoftaar TM, Wang D. A survey of transfer learning. Journal of Big Data. 2016; 3(1). doi: 10.1186/s40537-016-0043-6
31. Perez L, Wang J. The effectiveness of data augmentation in image classification using deep learning. Available online: https://arxiv.org/abs/1712.04621 (accessed on 11 January 2025).
32. Dong K, Zhou C, Ruan Y, et al. MobileNetV2 Model for Image Classification. Proceedings of the 2020 2nd International Conference on Information Technology and Computer Application (ITCA); 2020 doi: 10.1109/itca52113.2020.00106
33. Chen LC, Zhu Y, Papandreou G, et al. Encoder-decoder with atrous separable convolution for semantic image segmentation. Proc. ECCV; 2018.